Gas-phase catalysis by micelle derived Au nanoparticles on oxide supports

Ju Chou, Nathan R. Franklin, Sung-Hyeon Baeck, Thomas F. Jaramillo, and Eric W. McFarland*

Department of Chemical Engineering, University of California, Santa Barbara, CA 93106

Received 4 December 2003; accepted 18 March 2004

The reactivity of gold clusters (8–22 nm diameter) supported on different metal oxides (titanium dioxide (TiO_2), zinc oxide (ZnO), zirconium oxide (ZrO_2), and silicon dioxide (SiO_2)) was investigated in a continuous flow reactor. Clusters were encapsulated within polymer in toluene solution, impregnated onto the bulk supports, and reduced by calcination at 300 °C. Support dependent sintering ($TiO_2 > ZrO_2 > ZnO$) was observed following heating in air at 300 °C. For both CO oxidation and propylene hydrogenation, Au nanoclusters on TiO_2 exhibit the highest activity compared to other supports.

KEY WORDS: nanoparticles; catalysis; CO oxidation; propylene hydrogenation.

1. Introduction

Bulk gold has been considered catalytically inactive; however, gold nanoparticles (< 10 nm) have shown high activity for several types of oxidation and reduction reactions [1–7]. Several studies have documented the profound size dependent selectivity and low temperature activity of supported Au nanoparticles [6–10]. In particular, Haruta and colleagues showed data where Au clusters less than 2 nm were active for hydrogenation of propylene while clusters of 2–4 nm under the same conditions were selective for epoxidation [8,9]. Other work has verified the size dependence, albeit with somewhat different and unexplained product specificity [4]. What is clear is that to study and fully exploit Au nanoparticles for gas-phase catalysis, precise control and tuning of the nanoparticle size is desired.

Numerous methods for the preparation of Au nanoparticles have been employed including incipient wetness [11], deposition precipitation [2,8], organic capping [12] and micelle encapsulation [13–15]. Incipient wetness and deposition precipitation are very simple and scalable synthesis methods but suffer from several limitations such as precise particle size control and flexibility in oxide supports available for deposition, respectively. Organic capping has been employed with great success in producing Au nanoparticles with precise size control ($\pm 5\%$). The size distribution of particles produced depends on the combination of synthesis parameters used, with particular emphasis on concentration, temperature and the organic capping agent selected. This method is able to give a narrow distribution of size selected particles, but tuning of the particle size to a new size can require large modifications of the synthetic procedure; making it very difficult to differentiate changes in catalytic activity due to size dependent effects and those which are due to differences in the synthetic method. In this paper, a micelle encapsulation method based on block copolymers is used to synthesize Au nanoparticles. This method has been used previously with great success to produce a wide range of nanoparticles, with particle size defined by the length of the hydrophilic block of the polymer [13–15]. These particles are then typically deposited onto a planar substrate in a hexagonal pattern with the spacing defined by the length of the hydrophobic block of the copolymer. No previous work has investigated the activity of the clusters when used for gas-phase catalysis and here we have exploited the precise size control of the micelle derived clusters to prepare Au nanoparticle catalysts supported on different metal oxides where the cluster precursors are known to have a homogeneous distribution. The particles were deposited onto several different oxide supports and evaluated for catalytic activity and selectivity in CO oxidation and propylene epoxidation. In doing so we attempt to answer two questions: (1) Can micelle derived Au nanoparticles be active in gas-phase catalysis reactions? (2) Is the catalytic activity dependent on the specific support composition?

2. Experimental

$HAuCl_4 \cdot 3H_2O$, toluene, $CDCl_3$ were obtained from Sigma–Aldrich. Diblock copolymer [$polystyrene_{81,000}$-block-$poly(2\text{-vinylpyridine})_{14,200}$] was purchased from Polymer Source. Anatase TiO_2 (surface area 34.8 m^2/g) was donated by Saint–Gobain Norpro Corp. The other metal oxides including zinc oxide (ZnO), zirconium dioxide (ZrO_2) and silicon dioxide (SiO_2) were all obtained from Sigma–Aldrich.

*To whom Correspondence should be addressed.
E-mail: mcfar@engineering.ucsb.edu

1011-372X/04/0600–0107/0 © 2004 Plenum Publishing Corporation

2.1. Synthesis of catalyst

The micelles containing the gold nanoparticles were prepared as in Ref. [15]. Polymers were dissolved in toluene solution. The $HAuCl_4 \cdot 3H_2O$ diffuses gradually into the hydrophilic core of the micelle solutions. The micelles containing gold clusters precursors were then deposited onto different metal oxides by impregnation and the solvent was slowly evaporated in air during the impregnation process (figure 1). The dry sample was then ramped at 3 °C/min to 300 °C and held for 3 h to remove polymers surrounding the Au clusters as much as possible while minimizing particle size increases due to sintering. This process also serves to reduce the Au^{3+} at the core of the micelle to Au^0.

2.2. Catalyst characterization

The particle size of gold clusters was determined by transmission electron microscopy (TEM JEOL 2000FX) and high resolution TEM (JEOL 2010HR). The cluster sizes were determined by averaging the diameters of the clusters visualized within the TEM images and reported as the average diameter ±standard deviation. X-ray photoelectron spectra (XPS) were obtained on a Kratos Axis Ultra XPS system with a monochromatic Al–Kα source. SEM–EDS was collected by an FEI Co. XL30 Environmental Scanning Electron Microscope.

2.3. Reaction studies

The catalyst performance was measured in a packed bed reactor under atmospheric pressure. The reactor temperature was controlled over the range of 25–300 °C. The turn over frequency (TOF) was calculated from the TEM measured surface areas (assuming spherical shaped particles and that all surface atoms contribute to the activity).

The CO oxidation reaction mixture was composed of $CO : O_2 : Ar$ (1 : 1.5 : 10, vol ratio) with a total flow rate of 3000 mL/h, resulting in a space velocity of 20.8 mL/s-gcat for each sample. The CO oxidation reaction was monitored and analyzed *via* a two stage differentially pumped manifold and a quadrapole mass spectrometer (MS, Stanford Research Systems RGA 200).

The propylene reaction mixture was composed of $C_3H_8 : H_2 : O_2$ (1 : 1 : 1, vol ratio) with a total flow rate of 360 mL/h, resulting in a space velocity of 0.5 mL/s gcat. The propylene reaction products were monitored by MS, along with a cold trap for further analysis of trace products using NMR. Propylene oxide (PO) has structural isomers such as acetone and propanal which are difficult to distinguish using MS alone. However, they could be distinctively identified using NMR. A trap with $CDCl_3$ on an ice bath was used to collect organic products for NMR determination. The reaction products (at least 99%, a minute portion is sent to the MS) passed through the trap with $CDCl_3$ solvent, trapping all soluble products. The collected solutions were used for NMR determination to further identify the products of propylene reaction. ^{1}H-NMR spectra were collected on a Varian UNITY INOVA 400 MHz NMR Spectrometer at room temperature.

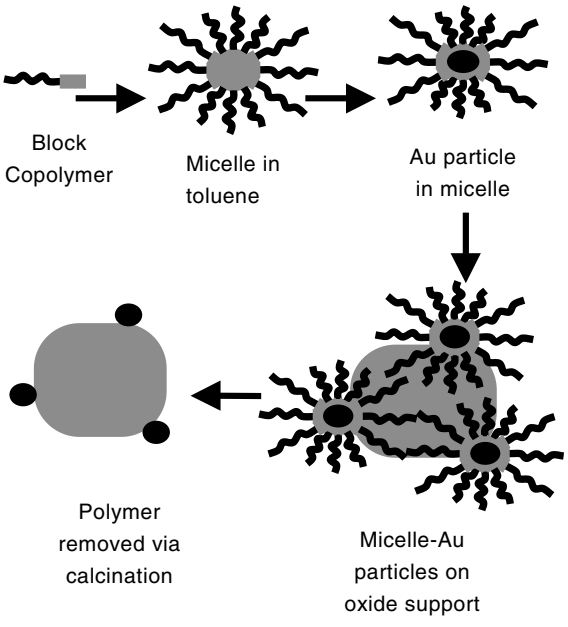

Figure 1. Catalyst preparation method

3. Results and discussion

3.1. Catalyst synthesis and characterization

Microscopy of the supported Au nanoclusters after calcination revealed the particle size distribution of the supported clusters. TEM of the clusters on TiO_2 after calcination showed the sizes to be 8.4 ± 1.6 nm (average ± standard deviation), figure 2a. Micelle solutions were also loaded onto other supports including ZnO, ZrO_2, and SiO_2. TEM of the Au clusters on ZnO after calcination is shown in figure 2b. Gold clusters were well dispersed on the ZnO surface after calcination, with particle sizes of 12.4 ± 2.5 nm. TEM of Au clusters on ZrO_2 after calcination is shown in figure 2c. Gold clusters were well dispersed on the ZrO_2 surface after calcination, with a size of 22 ± 2.0 nm. TEM was attempted for Au nanoparticles on SiO_2, however, due to the lack of contrast between the Au particles and the SiO_2 support, size determination was not possible.

The Au nanoparticle preparation method employed in this study was previously used to prepare Au nanoparticles deposited on planar substrates where the polymeric material was removed by oxygen plasma resulting in Au nanoparticles with an average size of 4.8 nm and a standard deviation of 1.3 nm [15]. We expected that the Au particles deposited on oxide

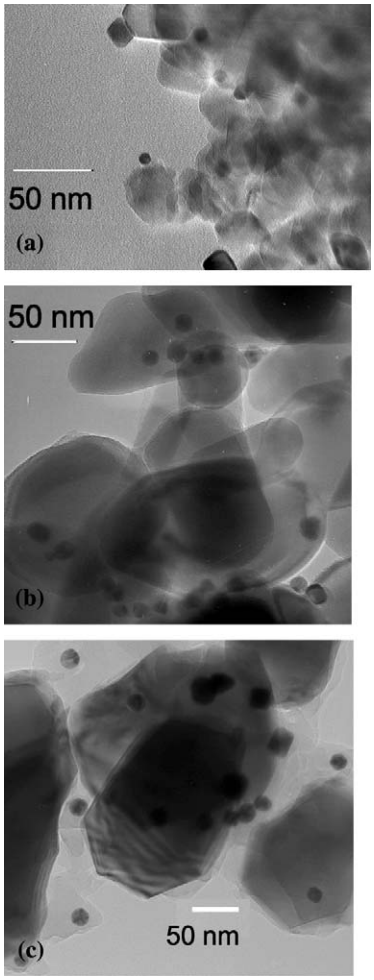

Figure 2. TEM images of Au nanoparticles on TiO_2 (a) ZnO (b) and ZrO_2 (c) after calcination.

supports would have similar size distributions. It was quite surprising to find that the particles were much larger than those previously observed, and that particle size was strongly dependent on the support composition.

XPS was used to determine the oxidation state of the gold before and after calcination. Figure 3 shows the Au-4f binding energy region for Au on TiO_2. The majority of the 4-f photoemission before calcination is assigned to Au^{3+} (84.8 and 88.5 eV). After calcination at 300 °C, the binding energies of Au-4f shifted to 83.4 and 87.1 eV which are assigned to the reduced metallic Au^0 [14,16]. The same change in Au oxidation states were observed for all other supports.

Composition of the catalysts was measured by Energy Dispersive Spectroscopy (EDS). We found small but detectable amounts of Cl present in the catalyst before and after calcination presumably due to the salt used in the preparation. The weight percent of Cl is estimated to be approximately 0.5%. The measured content of Au in the catalyst was roughly 1%, which supports the assumption that the 1% Au content target of the synthesis was achieved.

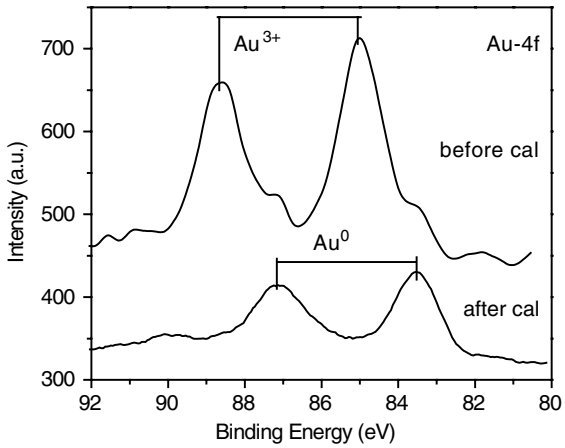

Figure 3. XPS of Au-4f in the Au/TiO_2 before calcination (upper curve) and after calcination (lower curve) at 300 °C for 3 h.

3.2. Support effects on CO oxidation

The influence of the support composition on the catalytic activity is shown in table 1. The clusters prepared from identical micelles supported on TiO_2, ZnO, ZrO_2 and SiO_2 and calcined identically were evaluated for CO oxidation under otherwise identical experimental conditions. Au clusters on TiO_2 showed the highest activity for CO oxidation while the clusters on SiO_2 were inactive. A strong interaction exists between TiO_2 and Au clusters, as the Au clusters showed negligible migration during the calcination. On other supports such as ZnO, the interaction between the support and Au clusters appears to be weaker than the case of TiO_2, as the Au clusters sintered during calcination and measured particle size grew substantially. Catalytic activity was observed to be much less than that of Au/TiO_2. On ZrO_2, the Au clusters are even larger than those on ZnO and this catalyst was found to be completely inactive up to 300 °C. Au clusters on SiO_2 were also found to be inactive for CO oxidation, however, previous researchers have observed small activity for the Au/SiO_2 system [17]. Given the observed

Table 1
Supports effects on the reactivity of CO + O_2 (T = 300 °C)

Support	Au particle size (nm)	TOF × 10^{-6} (mol CO/s g cat)	TOF[a] (s^{-1})
TiO_2	8.4 ± 1.6	19.2	1.3
ZnO	12.4 ± 2.5	4.8	0.4
ZrO_2	22 ± 1.2	0	0
SiO_2	Not measured	0	0

[a]TOF was calculated from $TOF = \gamma/n \cdot D.\gamma$ is the total moles of CO_2 converted per gram of gold per second; n is the total moles of gold at the surface; D is the cluster dispersion assuming cubo-octahedral clusters. D was obtained from Ref. [18] based on calculated total number of atoms in each cluster. The size of clusters was measured from TEM and we assumed spherical shape to calculate total number atoms in each cluster from radius of spheres.

size differences described above these results may not be unambiguously interpreted because different size Au particles were formed on each support, despite the fact that they were prepared identically.

3.3. Support effects on propylene reaction

The catalytic activity of gold catalysts from micelles was also investigated for reactivity with propylene. The propylene reaction was monitored by both MS and NMR. Figure 4 shows the mass spectrum traces/products in the reaction of propylene on Au/TiO_2 from micelles. When the temperature was increased, the intensity of mass 44 increased together with mass 43. Mass 44 can be attributed to either C_3H_8 or CO_2, however, CO_2 does not have a fragment at mass 43, thus the changes in mass 44 are most likely from C_3H_8. Nevertheless we could not rule out entirely trace production of CO_2 formation. Reaction products were also collected by a cold $CDCl_3$ trap for NMR determination. Figure 5 shows the ^{1}H-NMR spectrum of collected products in the $CDCl_3$ solvent. The chemical shifts at 1.7, 5.0 and 5.8 ppm are from the reactant gas of C_3H_6. The signals at 0.9 and 1.4 ppm are assigned to C_3H_8, which agrees with our assignment of mass 44 in MS data. These results suggest that 8 nm Au/TiO_2 is active for propylene hydrogenation. Trace amounts of PO were also detected by ^{1}H-NMR, though levels were too low to be detected using mass spectroscopy. The calculated conversion of propylene is 9.6% (TOF = 0.04 s^{-1}) and selectivity to propane (plus any CO_2) is 99%.

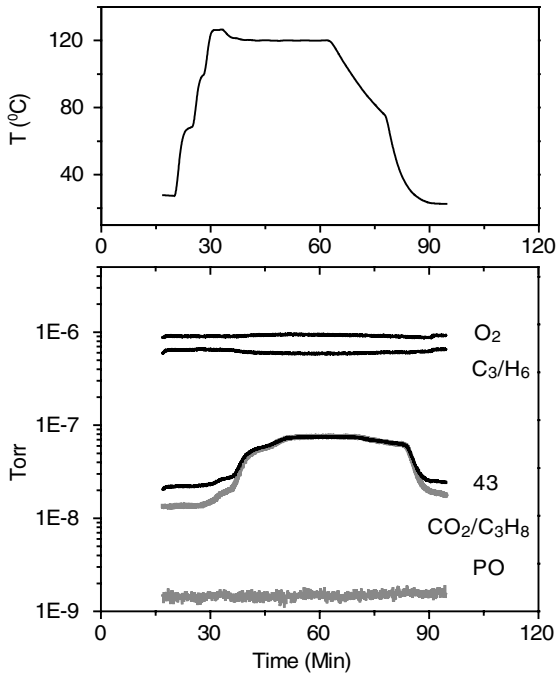

Figure 4. MS of propylene reaction products on Au/TiO_2. Species from the top are mass 32(O_2), mass 42(C_3H_6), mass 43(C_3H_8 fragment), mass 44(C_3H_8 or CO_2) and mass 58 (PO). Temperature changes during reaction are shown on the top.

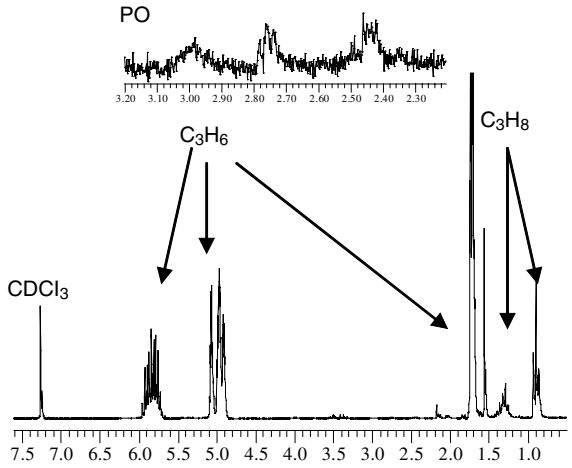

Figure 5. ^{1}H-NMR spectroscopy of products from propylene reaction on Au/TiO2. Products were trapped and collected in $CDCl_3$ solvent on an ice bath.

Au nanoclusters on the other supports such as ZnO, ZrO_2 and SiO_2 were also screened in the propylene reaction. For Au nanoparticles on these supports no propane or PO was observed by MS or NMR. Au/TiO_2 is found to have the highest activity for propylene hydrogenation, which correlates with the findings for CO oxidation.

The low temperature activity for hydrogenation on these ~8 nm Au clusters on TiO_2 is in contrast to the behavior observed by Haruta [8,9] who found that only the smallest clusters (~2 nm) are active for hydrogenation, and that the larger clusters were either active for epoxidation (~4 nm) or inactive (>4 nm) for either hydrogenation or epoxidation. The interesting and unexpected finding may be related to the presence of the Cl which was observed by EDS. The role of Cl^- is under investigation by our group.

4. Conclusion

Au nanoparticles have been prepared by micelle encapsulation and deposited onto several metal oxides supports including TiO_2, ZnO, ZrO_2, and SiO_2. Metallic gold was produced from Au^{3+} following calcination at 300 °C for 3 h in air. Au nanoparticles were well separated by the polymer chains and dispersed on the support after calcination, although some support dependent sintering was observed during calcination. The size dependent reactivity of Au nanoparticles on the different metal oxides is difficult to interpret due to sintering differences which resulted in different mean cluster sizes and, possibly, different size distributions on the different supports. In spite of this limitation, for both CO oxidation and propylene hydrogenation, Au/TiO_2 was found to be the most active Au catalyst among all the

metal oxide supports. This is most likely because the Au particles formed on TiO_2 were smaller than those formed on any other supports, and were in the range commonly associated with gold catalytic activity. Catalytically active Au nanoclusters can be prepared from micelles, however, the specific support material strongly influences the sintering behavior and the steady-state metal cluster size.

Acknowledgments

This research is supported by the US Department of Energy (DOE Grant #DE-FG03-8914048) and the AFOSR (Durint). Characterization made use of MRL Central Facilities supported by the MRSEC Program of the National Science Foundation under Award No DMR00-80034. The helpful discussions and advice of Dr. Beatriz Roldán Cuenya and Professor Galen Stucky are greatly appreciated.

References

[1] M. Haruta and M. Date, Appl. Catal. A 222 (2002) 427.
[2] Q. Fu, H. Saltsburg and M. Flytzani-Stephanopoulos, Science 301 (2003) 935.
[3] J.M.C. Soares, P. Morrall, A. Crossley, P. Harris and M. Bowker, J. Catal. 219 (2003) 17.
[4] M. Haruta, Catal. Today 36 (1997) 153.
[5] T.A. Nijhuis, B.J. Huizinga, M. Makkee and J.A. Moulijn, Ind. Eng. Chem. Res. 38 (1999) 884.
[6] T.V. Choudhary and D.W. Goodman, Top. Catal. 21 (2002) 25.
[7] M. Valden, X. Lai and D.W. Goodman, Science 281 (1998) 1647.
[8] T. Hayashi, K. Tanaka and M. Haruta, J. Catal. 178 (1998) 566.
[9] M. Haruta, Cattech 6 (2002) 102.
[10] P. Claus, A. Brückner, C. Mohr and H. Hofmeister, J. Am. Chem. Soc. 122 (2000) 11430.
[11] C. Mohr, H. Hofmeister, J. Radnik and P. Claus, J. Am. Chem. Soc. 125 (2003) 1905.
[12] B.L.V. Prasad, S.I. Stoeva, C.M. Sorensen and K.J. Klabunde, Langmuir 18 (2002) 7515.
[13] J.P. Spatz, S. Mössmer, C. Hartmann, M. Möller, T. Herzog, M. Krieger, H–G. Boyen, P. Ziemann and B. Kabius, Langmuir 16 (2000) 407.
[14] H.-G. Boyen, G. Kästle, F. Weigl, B. Koslowski, C. Dietrich, P. Ziemann, J. P. Spatz, S. Riethmüller, C. Hartmann, M. Möller, G. Schmid, M.G. Garnier and P. Oelhafen, Science 297 (2002) 1533.
[15] T.F. Jaramillo, S.H. Baeck, B.R. Cuenya and E.W. McFarland, J. Am. Chem. Soc. 125 (2003) 7148.
[16] M. Brust, M. Walker, D. Bethell, D.J. Schiffrin and R. Whyman, J. Chem. Soc. Chem. Commun. 7 (1994) 801.
[17] A. Wolf and F. Schüth, Appl. Catal. A 226 (2002) 1.
[18] J.M. Montejano-Carrizales, F. Aguilera-Granja and J.L. Moran-Lopez, NanoStruct. Mater. 8 (1997) 269.